Effects of Nb doping on the TiO_2 anatase-to-rutile phase transition

J. Arbiol,[a] J. Cerdà, G. Dezanneau, A. Cirera, F. Peiró, A. Cornet, and J. R. Morante
Department of Electronics, EME Electronic Materials and Engineering, University of Barcelona, Martí i Franquès 1, 08028 Barcelona, Spain

(Received 13 December 2001; accepted for publication 29 April 2002)

We study the influence of Nb doping on the TiO_2 anatase-to-rutile phase transition, using combined transmission electron microscopy, Raman spectroscopy, x-ray diffraction and selected area electron diffraction analysis. This approach enabled anatase-to-rutile phase transition hindering to be clearly observed for low Nb-doped TiO_2 samples. Moreover, there was clear grain growth inhibition in the samples containing Nb. The use of high resolution transmission electron microscopy with our samples provides an innovative perspective compared with previous research on this issue. Our analysis shows that niobium is segregated from the anatase structure before and during the phase transformation, leading to the formation of NbO nanoclusters on the surface of the TiO_2 rutile nanoparticles. © *2002 American Institute of Physics.* [DOI: 10.1063/1.1487915]

I. INTRODUCTION

Even since the first solid-state semiconductor gas sensors were produced, TiO_2 has been an important gas sensing material, mainly in lambda sensor devices, due to its dual response to both oxygen-rich and oxygen-lean atmospheres.[1–4] Its stability at temperatures up to 700 °C makes TiO_2 a suitable gas sensor material for harsh environments, such as the flue ducts of cars.[5–7]

TiO_2 can crystallize in different structures, rutile being the stable one. At low temperatures there is only a slight difference between the stability of rutile and the metastable anatase and brookite phases. Composition, *p*H, temperature, the rate of crystallization, and the structure of precursors may all determine the polymorph, but the reasons why these different phases are formed is poorly understood. For high temperature applications of titania as catalysts, membranes, and sensors, a stable anatase phase is necessary.[8] Therefore, one of the problems in both catalytic and sensor applications of anatase-based material is its transformation to rutile, a process that depends on both temperature and time.[9–11]

The presence of a suitable doping agent strongly affects the kinetics of this process. Indeed, some metal species can occupy interstitial positions or induce structural changes in metal oxide structures, as is the case of Nb, V, and Ce loaded onto TiO_2.[12–14] The effect of Nb doping in titania and its importance for oxygen sensors has recently been highlighted by several articles,[15–19] indicating higher device sensitivity[20] at lower working temperatures.[21,22] Likewise, recent studies have shown the feasibility of using Nb/TiO_2 as surface conductance CO sensors.[23] Moreover, Sberveglieri *et al.* found that Nb/TiO_2 thin films could be used to monitor methanol selectivity at ppm levels with negligible sensitivity to interfering gases, such as benzene and NO_2.[24] For both applications, nanosized grains of the sensing material are preferable in order to increase the area that is exposed to gases.

Although many articles mention the influence of Nb on strain, grain size evolution, and anatase-to-rutile transformation, as well as the consequences for sensing devices,[17,19,20,25,26] little systematic research has been carried out in this field. Therefore, our work provides useful data for the technological improvement of TiO_2-based gas sensor devices, as well as for the scientific understanding of the anatase-to-rutile transformation and the role of Nb doping in these mechanisms.

This article presents a complete study of the influence of Nb on the TiO_2 phase transition from the anatase metastable phase to the rutile stable phase. The analysis was carried out using Raman spectroscopy and x-ray diffraction (XRD). The use of transmission electron microscopy (TEM) enabled us to analyze TiO_2 grain size evolution with Nb content at different annealing temperatures, as well as Nb segregation.

II. EXPERIMENTAL DETAILS

Nb-doped samples were synthesized by induced laser pyrolisis, with various Nb contents ranging from undoped to 24.5 Nb/Ti at. % (Table I), following the procedure described elsewhere.[27] Briefly, a CO_2 laser beam perpendicularly intersects a reactant stream, defining a well-localized reaction zone that enables the growth of nanometric powders with a narrow size distribution. Ti–isopropoxide vapors were used for the synthesis of pure TiO_2, while controlled amounts of Nb–isopropoxide vapors were added to the reactant stream for the production of Nb–Ti oxides. All these raw samples were subjected to annealing temperatures ranging from 600 to 900 °C, in steps of 50 °C. The thermal treatment applied in all the series was a heating ramp of 10 °C/min to the holding temperature for 2 h, followed by free cooling, the whole process being carried out under atmospheric air.

XRD was performed on a Siemens D5000 diffractometer working with the Cu $K_{\alpha 1,2}$ wavelength. Data were collected in steps of 0.05° from 20° to 60° in 2-θ. Raman spectra were recorded on a Jobin–Yvon T6400 instrument, with an Ar^+ laser source of 514 nm wavelength and an incident power of 2 mW/mm^2. TEM was carried out using a Phillips CM30

[a]Author to whom correspondence should be addressed; electronic mail: arbiol@el.ub.es, http://nun97.el.ub.es/~arbiol

TABLE I. Description of sample metal loading concentrations and annealing temperatures applied in each set.

Samples	Nb/Ti (at. %)	$T_{annealing}$ (°C)
A	0.0	600–900
B	2.9	600–900
C	3.4	600–900
D	10.9	600–900
E	24.5	600–900

SuperTwin electron microscope operated at 300 keV with 0.19 nm point resolution. For TEM observations, Nb/TiO_2 nanopowders were ultrasonically dispersed in ethanol and deposited on amorphous holey carbon membranes.

III. RESULTS

Both the Nb content and the annealing temperatures influenced the percentage of anatase and rutile phases present in the samples. For example, the evolution of Raman spectra as a function of annealing temperature for samples A, B, and E is shown in Figs. 1(a)–1(c), respectively. On these figures, we have marked the main characteristic peaks of anatase at 198 cm^{-1} (E_g), at 397 cm^{-1} (B_{1g}) and 516 cm^{-1} (B_{1g}), 639 cm^{-1} (E_g), and of rutile at 235 cm^{-1} (disorder or second order scattering),[28] 449 cm^{-1} (E_g), and 610 cm^{-1} (A_{1g}).[29] The Raman spectra show that the presence of different Nb percentages influences the phase transition rate. Similarly, XRD patterns for samples A, B, and E [see Figs. 2(a)–2(c), respectively] show a clear evolution of TiO_2 with different anatase-to-rutile ratios.

In order to quantify the anatase-to-rutile transformation, XRD peak intensity ratios were used (Fig. 3). The ratio between anatase and rutile extracted from XRD spectra was computed with the empirical relationship used by Depero *et al.*[19]

$$R(T)=0.679\frac{I_R}{I_R+I_A}+0.312\left(\frac{I_R}{I_R+I_A}\right)^2, \quad (1)$$

where $R(T)$ is the percentage content of rutile at each temperature, I_A is the intensity of the main anatase reflection (101) ($2\theta=25.30°$), and I_R is the intensity of the main rutile reflection (110) ($2\theta=27.44°$).

The 50% molar anatase and rutile mixture point is marked with a dashed line (Fig. 3). Comparing results, and taking this point to be one of the most characteristic in the anatase-to-rutile transformation, we found that sample A, which contains no Nb, reached the 50% anatase/rutile point at around 700 °C, and this quickly evolved into a complete rutile transformation. At 750 °C sample A had reached 90% of rutile content.

In the case of the lowest loaded samples (B and C), 50% of the rutile transformation did not occur until temperatures above 850 °C, and even at temperatures as high as 900 °C the samples continued to contain a significant anatase part (up to 25% molar in the case of sample B and 20% in the case of sample C).

For the highest loaded samples we found that the 50% molar anatase and rutile mixture was obtained at around

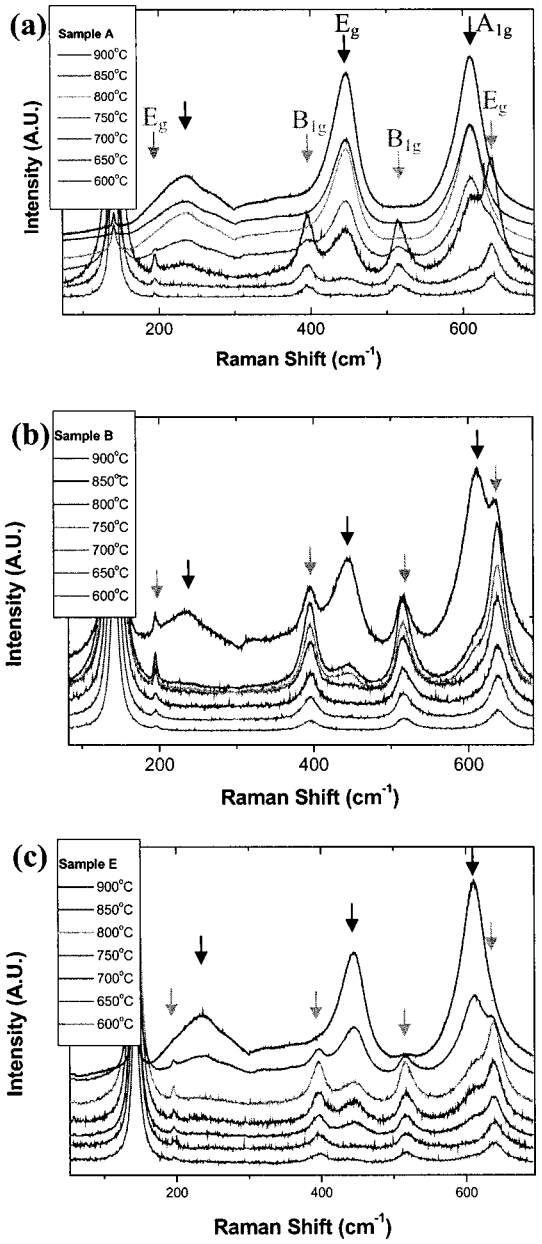

FIG. 1. (a)–(c) RAMAN spectra of samples A, B, and E, respectively, at various temperatures (600–900 °C). Notice the anatase-to-rutile transition when the annealing temperature is increased. Anatase and rutile main peaks are marked with gray and black arrows, respectively.

800 °C and 825 °C for samples E and D, respectively. Moreover, for high annealing temperatures (900 °C), we obtained around 85% and 90% of the rutile transformation for samples D and E, respectively.

The evolution of the phase transformation was also analyzed by means of selected area electron diffraction (SAED). As an example, the qualitative results obtained by SAED for the samples at high (900 °C) annealing temperatures are shown (Fig. 4), and these results can be directly compared with those obtained by means of XRD and Raman. From our SAED patterns, the rings and spots present are identified in order to determine the crystal phase to which they correspond. Notice that the rings and spots analyzed are marked in the diffractograms using a symbolic notation: circles marked

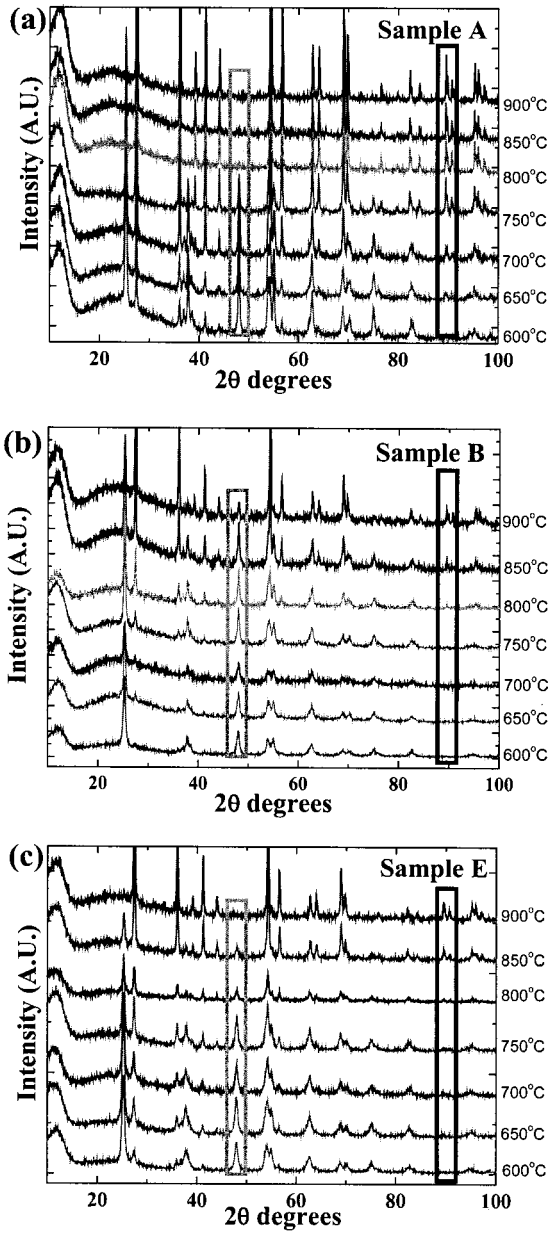

FIG. 2. (a)–(c) XRD spectra of samples A, B, and E, respectively, at various temperatures (600–900 °C). Gray and black selections show the evolution of anatase and rutile peaks, respectively.

1–5 (TiO_2 anatase) and circles marked A–D (TiO_2 rutile). The existence of a few diffuse spots that do not correspond to any of the former phases, suggests there is an additional phase related to the presence of Nb (circles marked i–iii). After indexing these spots, we compared the data obtained with those shown in JCPDS cards for the different Nb oxide phases, as well as the known alloys composed of Nb and Ti. The crystal phases considered were those corresponding to: NbO,[30] NbO_2,[31] β-NbO_2,[32] Nb_2O_5,[33] and $TiNb_2O_7$.[34] After comparing tabulated and experimental data, we found that the above-mentioned diffuse spots are in good agreement with the NbO phase. It should be pointed out that the presence of strong and well-defined spots is due to the important increase in grain size of the TiO_2 nanopowders at such high temperatures. This is the case for the sample A900 pattern,

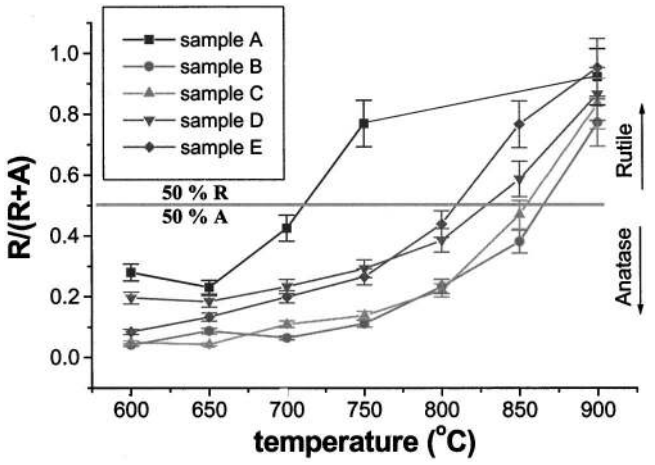

FIG. 3. Anatase-to-rutile phase transition evolution with respect to temperature for samples A–E. Data obtained from XRD results using Depero *et al.* empirical relationship (Ref. 19).

and, to a lesser extent samples D900 and E900. The main phase in these three samples is clearly rutile. However, the SAED patterns corresponding to B900 and C900 still have an important anatase content and NbO diffuse spots can also

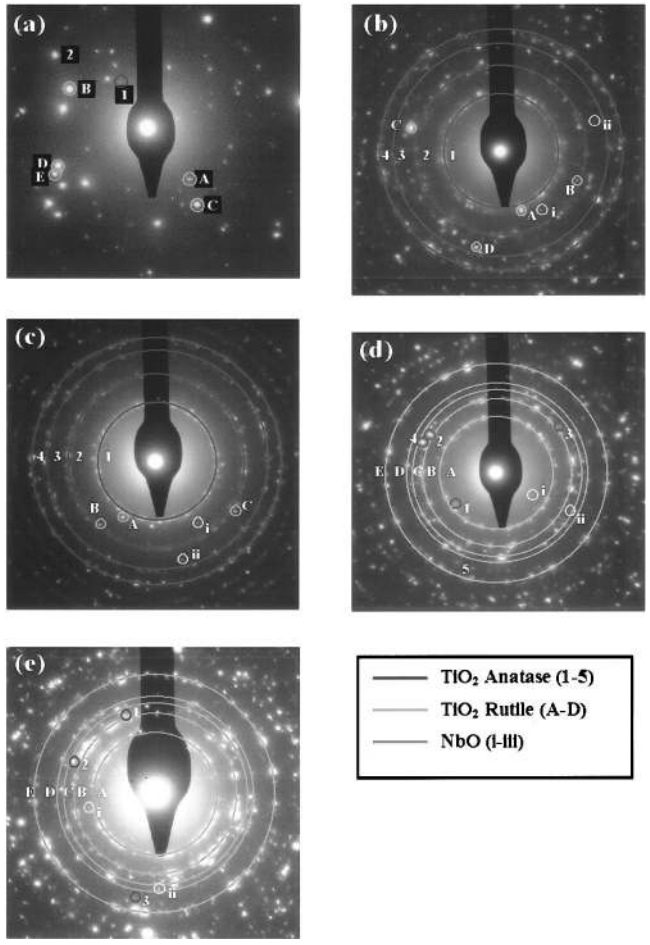

FIG. 4. SAED patterns corresponding to samples: (a) A900, (b) B900, (c) C900, (d) D900, and (e) E900. Rings and spots analyzed have been marked in the diffractograms using the following notation: circles marked 1–5 (TiO_2 anatase), circles marked A–D (TiO_2 rutile) and, finally, circles marked i–iii (the NbO phase).

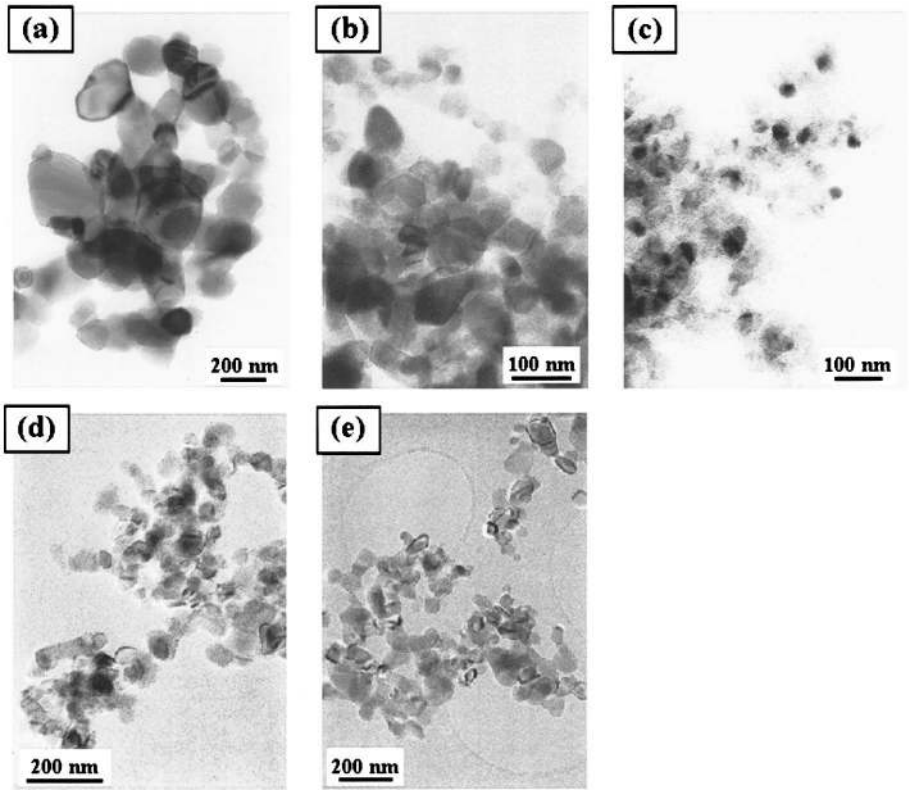

FIG. 5. General TEM view of samples: (a) A900, (b) B900, (c) C900, (d) D900, and (e) E900.

be seen in them.

The TiO_2 grain size evolution of our samples was analyzed by means of TEM. Figure 5 shows a set of TEM bright field micrographs corresponding to the samples annealed at high temperature (900 °C). Their respective grain size histograms are also given in Fig. 6. The statistics computed from the histograms show a noticeable change in grain size that depends on the Nb loading values. All mean grain size results are summarized in Table II and in Fig. 7. A dramatic decrease in nanoparticle size occurred when samples were loaded with a low percentage of Nb. The mean particle size had a minimum value of around 2%–3% Nb atomic percentage, and then slowly increased as the Nb loading was also increased. It is important to note that the mean grain size is closely related to the amount of rutile phase present in the samples. In general, the more rutile percentage found in our samples, the bigger the mean grain size.

High-resolution TEM (HRTEM) and digital image processing (DIP) were used to complete the sample analysis. HRTEM analysis of the sample nanopowders annealed at low temperatures (600 °C) revealed no Nb clusters or Nb alloys around the TiO_2 anatase nanoparticles [Fig. 8(a)].

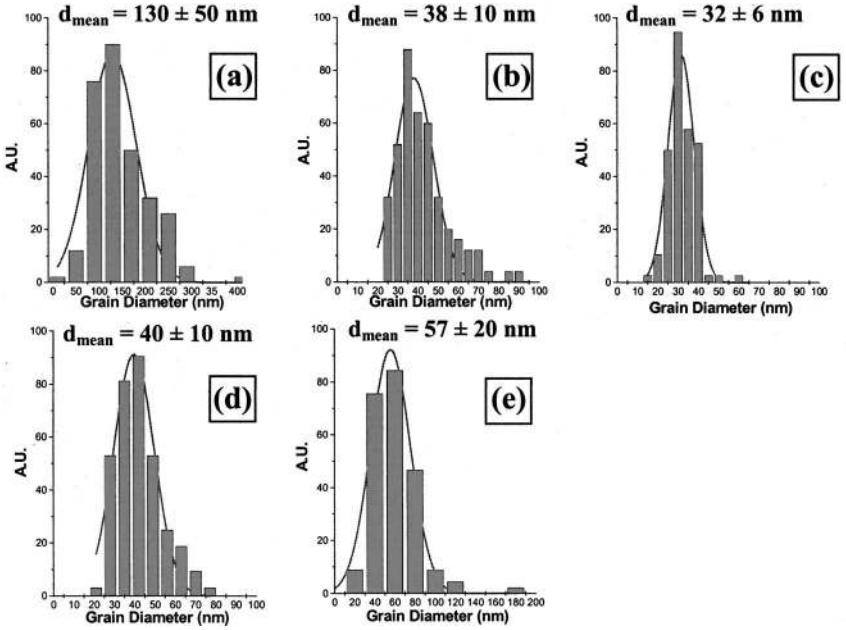

FIG. 6. Grain size histograms corresponding to each sample: (a) A900, (b) B900, (c) C900, (d) D900, and (e) E900.

TABLE II. Mean nanopowder diameters obtained from grain size histograms after Gaussian fit.

A600 D (nm)	B600 d (nm)	C600 d (nm)	D600 d (nm)	E600 d (nm)	A900 D (nm)	B900 d (nm)	C900 d (nm)	D900 d (nm)	E900 d (nm)
20±8	16±4	14±3	13±2	12±4	130±50	38±10	32±6	40±10	57±20

However, despite not being shown by TEM, electron dispersive x-ray spectroscopy (EDS) analysis [Fig. 8(b)] of the nanoparticles confirmed that the grains with anatase structure do contain Nb atoms, as expected.

HRTEM showed that Nb is segregated from the anatase structure just before or even during the phase transformation to rutile. The segregated Nb was always found in its NbO oxidized phase, forming nanoclusters on the surface of TiO_2 rutile grains (Fig. 9), and followed a Volmer–Weber growing mode until clusters merged into a thin NbO film for high loading values (Fig. 10). The HRTEM distribution pattern of the Nb inside the anatase nanograins and the segregated suggests that Nb segregation may be closely related to inhibition of the anatase-to-rutile phase transition, as observed by XRD, Raman, and SAED.

When anatase is transformed to rutile, Nb atoms are segregated from the rutile stable phase grains, thereby creating a thin NbO film (in the case of high Nb loadings) or small nanoclusters (in the case of lower Nb loadings). At an intermediate stage, an anatase layer, which still contains Nb atoms, remains at the exterior surface until the total transformation to rutile phase.

Figure 10(a) shows a scheme of the proposed phase transition mechanism, frozen at an intermediate stage. The model was created using the RHODIUS software package.[35] In this model we took the bulk of a pure TiO_2 rutile particle covered by a few monolayers of NbO, with a thin anatase film on top. In order to validate our previous results, we used electron microscopy simulation (EMS) software to compute the HRTEM image of this model. Similar contrast patterns and the same plane spacing distances were obtained when comparing the HRTEM-simulated images [Fig. 10(b)] with those obtained experimentally [Fig. 10(c)]. The simulated image was obtained under the following microscope conditions: 300 kV and $C_s = 1.2$ mm, layer thickness = 40 nm, and defocus = 60 nm; the simulated image was obtained 10° off the [001] TiO_2 rutile zone axis. It is normally expected that phase transition is too fast to be observed, and this is indeed the case for our samples: rutile or anatase nanoparticles, but never mixed phases in the same grain. Nevertheless, the observation of frozen nanoparticles and the correlation with simulation experiments provides further insight into phase transition phenomena.

In summary, all our results, both the spectroscopic (Raman and XRD) and SAED show an important inhibition of the TiO_2 anatase-to-rutile phase transition when Nb is introduced into the samples. These results are supported by HRTEM, finding that the number of anatase nanoparticles is much higher for those samples which contain Nb. In order to

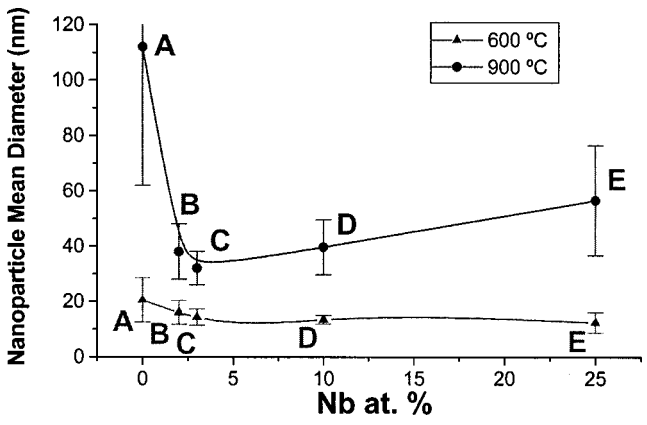

FIG. 7. Grain size evolution at low (600 °C) and high (900 °C) annealing temperatures.

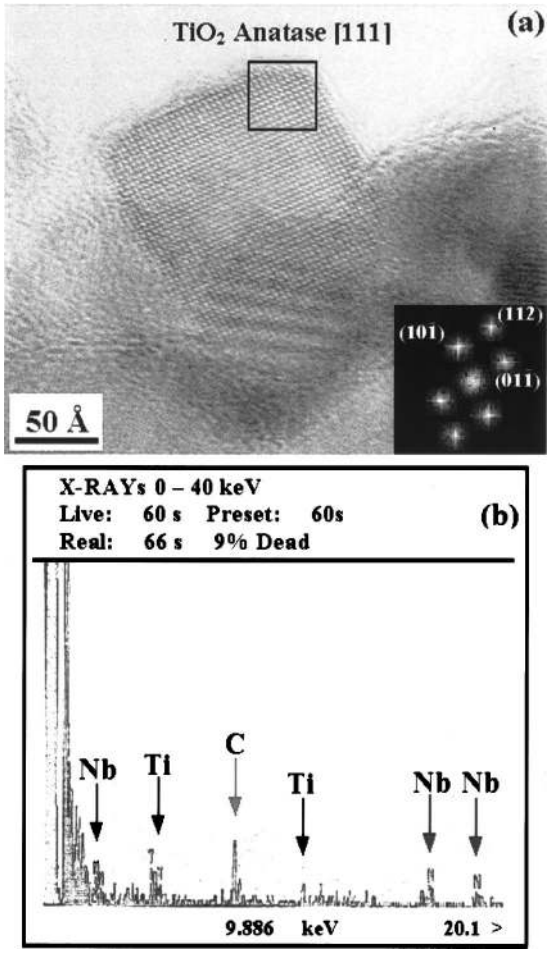

FIG. 8. (a) HRTEM micrograph showing a rectangular anatase nanoparticle. A digital diffractogram of the squared region is also shown, allowing us to determine the atomic structure of the selected grain. (b) EDS spectrum corresponding to the area shown in (a). The presence of Nb atoms is clear although the signal is weak. Titanium also shows two peaks. While Cu is also present, this last signal comes from the x ray scattered in the copper grid.

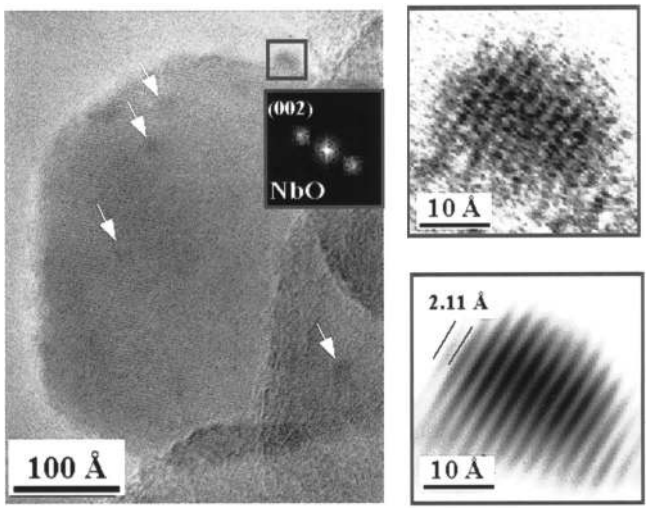

FIG. 9. HRTEM micrograph of D900 sample. White arrows indicate some of the NbO nanoclusters segregated on the TiO_2 rutile surface. The squared details show the DIP analysis of a NbO nanocluster.

understand the influence of niobium in the phase transition mechanism several aspects have to be taken into account. An explanation of the phase transition inhibition phenomena is proposed in Sec. IV.

IV. DISCUSSION

A. Background

On the basis of phase equilibrium experiments, natural abundance and atomistic simulations, it has been widely believed that only rutile has a true field of stability at low pressure, while anatase is metastable with respect to rutile. Furthermore, the defect structure of both phases has been extensively studied, but there are no available data regarding the energy cost of such a defect formation in either structures. The defects generally encountered in TiO_2 are oxygen vacancies, interstitial or substitutional Ti^{3+} ions, interstitial Ti^{4+} ions and cation vacancies. The tolerance of anatase and rutile toward the presence of such defects can be qualitatively correlated with the local environment of titanium and to elastic properties. In both structures Ti is sixfold coordinated, but the number of shared octahedral edges increases from two in rutile to four in anatase. Traditional crystal chemical theory argues that shared edges should lead to cation–cation repulsion and structural destabilization, in accordance with the relative stability of both phases. In addition, it also suggests that the presence of a cation vacancy should be better tolerated in anatase structure, due to a better charge defect compensation by neighboring Ti cations. Experimental results[36] confirm this latter hypothesis since anatase and rutile, prepared from the same solution and heat treated at 600 °C, present 20% and 10% of cation vacancies, respectively. The high value of rutile bulk modulus (210 GPa)[37] compared with that of anatase (178 GPa),[38] which reflects the curvature of the potential function, also suggests that the introduction of sterically costing defects in rutile would imply a higher energy per defect than in the case of anatase.

As in the case of undoped TiO_2, the tolerance of anatase and rutile structures to Nb doping may be described qualitatively. First, the similarity of Nb^{+5} ($r=0.70$ Å) and Ti^{+4} ($r=0.68$ Å) radii in sixfold coordination suggests that the solubility of niobium in TiO_2 phases will depend mainly on the charge compensation mechanism rather than on the induced stress. Thus, whatever the structure considered, the effect of introducing Nb is given by the following charge

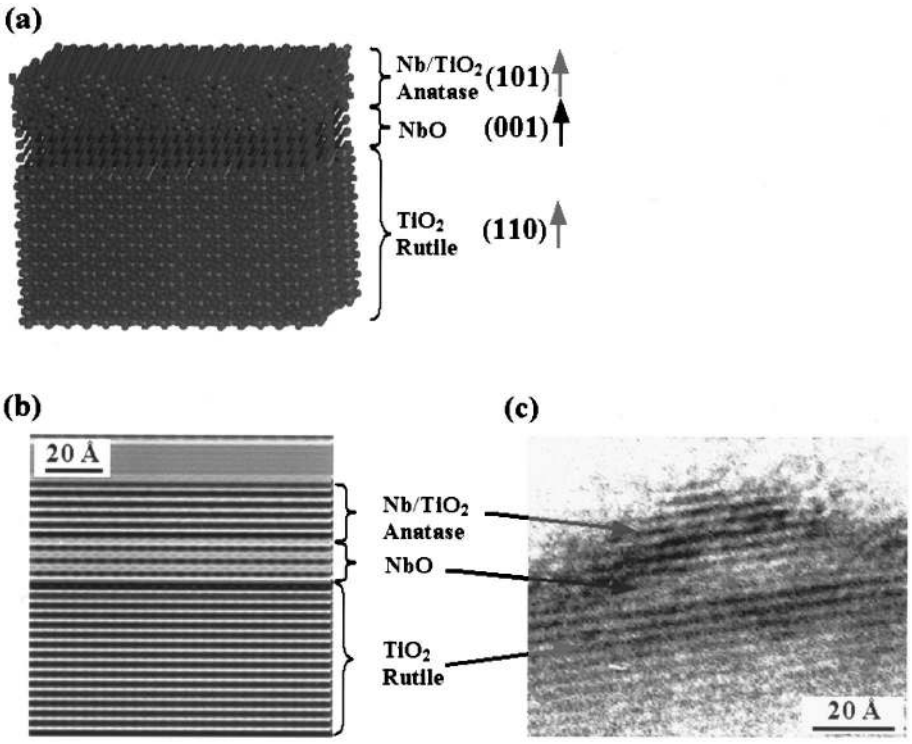

FIG. 10. (a) Supercell model reproducing the growth mechanism. Phase transition occurs from inside to outside at the same time as Nb is segregated from anatase when this is transformed into rutile. (b) Computer image simulation of the model shown in (a); notice the good resemblance of contrast lines to those shown in the HRTEM micrograph in (c).

equilibrated equations, expressed in classical Kröger–Vink notation:

$$\tfrac{1}{2}Nb_2O_5 + Ti_{Ti}^{x} \rightarrow Nb_{Ti}^{\bullet} + \tfrac{1}{4}V_{Ti}^{''''} + TiO_2 + \tfrac{1}{4}O_2, \quad (2)$$

$$\tfrac{1}{2}Nb_2O_5 + Ti_{Ti}^{x} \rightarrow Nb_{Ti}^{\bullet} + Ti_{Ti}^{\prime} + \tfrac{5}{4}O_2, \quad (3)$$

where the charge compensation of Nb^{5+} is achieved either by the creation of one vacancy per titanium site per four Nb introduced, or by the reduction of one Ti^{4+} in Ti^{3+} per Nb introduced. Both mechanisms may be present, the latter being much more likely to occur at high temperatures. Whatever the case, the presence of a vacancy on a titanium site or the stress induced by the presence of Ti^{3+}, suggests that a higher solubility limit of niobium into TiO_2 may be found in anatase than rutile, in line with the previous discussion for nondoped TiO_2. However, for a complete description of possible Nb-doped TiO_2 defects, the occurrence of oxygen vacancies also has to be considered. It would be expected that the introduction of niobium will reduce the amount of oxygen vacancies, due to it having a higher positive charge than titanium.

B. Inhibition of the anatase-to-rutile phase transition

During phase transformation, the anatase pseudoclose-packed planes of oxygen {112} are retained as rutile close-packed planes {110} and a cooperative rearrangement of the titanium and oxygen ions occurs within this configuration.[39] The oxygen vacancies placed in anatase planes act as nucleation sites for the anatase-to-rutile phase transformation.[40]

If we consider defect formation by foreign ions in titania lattice, it can be supposed that ions, which enter into the system substituting Ti^{4+}, may either enhance or delay the transformation from anatase to rutile depending on whether the number of oxygen vacancies is increased or decreased.[25] When niobium ions enter substitutionally into TiO_2, the charge of the Nb^{5+} ions should be compensated for a decrease in oxygen vacancies, leading to the hindering of the anatase-to-rutile transformation.[25,41]

C. Grain growth inhibition

An important inhibition of grain growth was observed at high annealing temperatures (900 °C) when Nb was introduced into our samples. The TEM results and particle size histogram clearly show an inflexion point at which inhibition reaches a maximum. This point was found to be around 3–4 at % Nb, where the mean TiO_2 nanoparticle size was around 32 nm. This latter value greatly increased for both the unloaded sample (up to 130 nm) and the high loaded samples (up to 57 nm). In general terms, the grain growth hindering observed when our samples were loaded with Nb was very similar to that found by other authors.[20,42] The Nb^{5+} radius (0.70 Å) is slightly bigger than the Ti^{4+} radius (0.68 Å) and this means that Nb^{5+} induces slight stress in titania lattice, which may hinder the growth of the TiO_2 crystallites, as was found by Sharma and Bhatnagar.[20] Moreover, we also found that TiO_2 anatase particles were smaller than rutile ones in the same sample. These phenomena as well as the existence of an inflexion point in grain growth are discussed below when the effects of Nb segregation have been introduced.

D. NbO segregation during phase transition

As was demonstrated by HRTEM analysis, niobium is segregated from the TiO_2 structure. This segregation has two possible origins: segregation during phase transition and/or segregation at high loading values. When might this occur? The above explanations suggest that it would be very difficult for an anatase grain containing Nb dopants to transform to rutile. Therefore, it is possible that transformation is accompanied by prior Nb segregation, in order to allow an increase in oxygen vacancies in our material and thus facilitate phase transition. The process described could explain the behavior of our anatase nanoparticles when temperature was increased; Nb^{5+} ions would remain inside anatase bulk until the temperature was high enough to provide the mobility necessary for our niobium ions to sinter. Thus, the Nb aggregates created would be expelled from the anatase structure and be placed on the TiO_2 surface in an oxidized Nb phase. At the same time, once the main part of the niobium has left the anatase structure, a fast transformation to rutile would occur, since at such high temperatures phase transition would be highly favored.

If we consider Nb segregation on the TiO_2 surface, it would be expected that Nb would react with the TiO_2 surface and acquire one of its oxidized phases, which are thermodynamically more stable than the metallic ones. Recently, Marien *et al.*[43] used a simple model to calculate the change in Gibbs free energy ΔG^o of the surface reaction, assuming that TiO_2 (rutile) was reduced to Ti_2O_3

$$2TiO_2 + Nb \rightarrow Ti_2O_3 + NbO \quad (\Delta G^o = -36\ \text{kJ/mol}), \quad (4)$$

$$4TiO_2 + Nb \rightarrow 2Ti_2O_3 + NbO_2 \quad (\Delta G^o = -57\ \text{kJ/mol}), \quad (5)$$

$$10TiO_2 + 2Nb \rightarrow 5Ti_2O_3 + Nb_2O_5 \quad (\Delta G^o = -59\ \text{kJ/ml}). \quad (6)$$

After analyzing their specimens, they were unable to determine whether NbO, NbO_2, or Nb_2O_5 was formed. As can be seen, a most favorable reaction, thermodynamically speaking, would transform Nb into Nb_2O_5, due to its lower Gibbs free energy value. Controversially, our SAED and HRTEM results suggest the presence of NbO clusters on TiO_2 grain surfaces.

After analyzing a few hundred TiO_2 nanoparticles we found no anatase nanoparticle with NbO clusters on its surface. Conversely, the niobium EDS signal comes from anatase bulk, meaning that the anatase structure enabled Nb atoms to be incorporated within it. However, the presence of NbO clusters on the surface of rutile grains would confirm our hypothesis that there is a prior segregation of Nb ions before or during phase transition.

In this work we have related the segregation of Nb to the anatase-to-rutile phase transition.

E. NbO segregation at high Nb loading values

So far, we have shown that the segregation of Nb ions from the anatase structure favors the anatase-to-rutile phase

transition. It has been pointed out that this segregation is possible when a certain annealing temperature is reached. However, there is another effect, which has yet to be explained, namely, the acceleration of phase transformation for high as opposed to low loading values. The phase transition rate would be expected to decrease when Nb loading was increased but, as our experimental results show, there is an inflexion point at around 3–4 at % Nb, after which the transformation rate slowly increases again as niobium loading is also increased.

Taking into account the stress induced in the anatase grains by the diffusion of Nb ions inside its structure, we suggest that there is a point at which the excess of stress is not thermodynamically supported, and the structure would therefore reduce it by removing part of the Nb ions. At this point, the solubility limit of the Nb in the TiO_2 anatase structure would be reached, and the excess of Nb ions would be segregated from the grain. In this case, niobium segregation would occur earlier than in the grains from low loaded samples, thus explaining the faster transformation to rutile of high loaded samples.

Moreover, in the case of the highest loaded sample (24.9 at % Nb), NbO seemed to create a thin film composed of a few monolayers on TiO_2 rutile grain surfaces. On the basis of our HRTEM observations, it seems that NbO may follow a Volmer–Weber growing mode on the TiO_2 surface,[44,45] forming three-dimensional clusters until the quantity of material is sufficient for the clusters to merge into a thin film.

To sum up, the general phase transition and growth mechanism proposed would be the following:

(1) The presence of Nb substitutional ions in the anatase structure hinders or inhibits the phase transition and growth of nanopowders.
(2) When the annealing temperature is increased, the Nb ions are segregated from the grains, forming oxidized species (we found NbO forming clusters on grains surfaces). This segregation would be enhanced when increasing the metal loading percentage, due to the higher stress introduced in the anatase structure.
(3) Once part of this Nb is outside the anatase structure, the number of oxygen vacancies would be recovered in order to ensure crystal charge neutrality; and this would favor the anatase-to-rutile phase transition. At the same time, the reduction in the stress induced by Nb ions would favor grain growth, leading to the formation of bigger TiO_2 rutile nanoparticles, as observed by HRTEM.

V. CONCLUSIONS

We have shown that there is a close relationship between grain growth and the anatase-to-rutile phase transition. Both mechanisms are hindered due to the presence of niobium ions inside anatase bulk, so both will be favored after Nb segregation. Thus, the undoped sample is the one whose TiO_2 nanoparticles experience a faster phase transition and growth. This would be followed by the high loaded samples, in which a relatively fast segregation of part of the Nb would also favor fast transition and growth, and finally, the TiO_2 grains from low loaded samples, which would maintain Nb ions in the anatase structure until they reach a high annealing temperature. Nb segregated from TiO_2 nanoparticles was always found in its NbO oxidized phase, forming nanoclusters on the grain surface and following a Volmer–Weber growing mode until clusters merge into a thin film for high loading values.

In light of the experimental results obtained, we have also proposed a model of phase transition and growth mechanisms in Nb/TiO_2 nanostructured systems.

ACKNOWLEDGMENTS

This work has been partially funded by the EU INCO Project No. ICA2-CT-2000-10017 and by the Spanish CICYT program Contract No. MAT 99-0435-C02-01. The authors would also like to acknowledge CISE (Italy) for supplying the raw set of Nb/TiO_2 samples.

[1] T. Y. Tien, H. L. Stadler, E. F. Gibbons, and P. J. Zacmanidis, Ceram. Bull. **54**, 280 (1975).
[2] W. Göpel and R. Rocker, Phys. Rev. B **28**, 3426 (1993).
[3] U. Kirner, K. D. Schierbaum, W. Göpel, B. Leibold, N. Nicoloso, and W. Weppner, Sens. Actuators B **1**, 103 (1990).
[4] M. Ferroni, V. Guidi, G. Martinelli, G. Faglia, P. Nelli, and G. Sberveglieri, Nanostruct. Mater. **7**, 709 (1996).
[5] T. Akio, M. Toshitaka, and K. Nobuo, US Patent No. 54656863 (1987).
[6] R. G. Fournier, C. A. Valdes, and J. K. Chandra, US Patent No. 55776601 (1998).
[7] K. Fukaya and M. Yamauchi, US Patent No. 2001/0017057 (2001).
[8] G. Deo, A. M. Turek, I. E. Wachs, T. Machej, J. Haber, N. Das, H. Eckert, and A. M. Hirt, Appl. Catal., A **91**, 27 (1992).
[9] P. K. Dutta, A. Ginwalla, B. Hogg, B. R. Patton, B. Chwieroth, Z. Liang, P. Gouma, M. Mills, and S. Akbar, J. Phys. Chem. B **103**, 4412 (1999).
[10] C. Suresh, V. Biju, P. Mukundan, and K. G. K. Warrier, Polyhedron **17**, 3131 (1998).
[11] M. Ferroni, M. C. Carotta, V. Guidi, G. Martinelli, F. Ronconi, O. Richard, D. Vandyck, and J. Vanlanduyt, Sens. Actuators B **68**, 140 (2000).
[12] D. Mardare and P. Hones, Mater. Sci. Eng., B **68**, 42 (1999).
[13] Y. Gao, Thin Solid Films **346**, 73 (1999).
[14] S. Matsushima, Y. Teraoka, N. Miura, and N. Yamazoe, Jpn. J. Appl. Phys., Part 1 **27**, 1798 (1988).
[15] J. Zhu, C. Ren, G. Chen, C. Yu, J. Wu, H. Mu, Sens. Actuators B **32**, 209 (1996).
[16] K. Zakrzewska, M. Radecka, M. Rekas, Thin Solid Films **310**, 161 (1997).
[17] R. K. Sharma, M. C. Bhatnagar, and G. L. Sharma, Sens. Actuators B **46**, 194 (1998).
[18] Z. Jianzhong, R. Congxin, C. Guoliang, M. Haichuan, W. Jiali, and Y. Chunying, Sens. Actuators B **46**, 180 (1998).
[19] L. E. Depero, L. Sangaletti, B. Allieri, E. Bontempi, R. Salari, M. Zocchi, C. Casale, and M. Notaro, J. Mater. Res. **13**, 1644 (1998).
[20] R. K. Sharma, M. C. Bhatnagar, Sens. Actuators B **56**, 215–219 (1999).
[21] R. K. Sharma, M. C. Bhatnagar, and G. L. Sharma, Appl. Surf. Sci. **92**, 647 (1992).
[22] M. Z. Atashbar, H. T. Sun, B. Gong, W. Wlodarski, and R. Lamb, Thin Solid Films **326**, 238 (1998).
[23] M. Ferroni, O. Richard, N. Bonini, M. C. Carotta, V. Guidi, G. Martinelli, F. Roncani, D. Van Dyck, and J. Van Landuyt, Proceedings of the 13th European Conference on Solid-State Transducers, 1999.
[24] G. Sverglieri, E. Comini, G. Faglia, M. Z. Atashbar, and W. Wlodarski, Sens. Actuators B **66**, 139 (2000).
[25] M. K. Akhtar and S. E. Pratsinis, J. Am. Ceram. Soc. **75**, 3408 (1992).
[26] E. Cominia, G. Faglia, G. Sberveglieri, Y. X. Li, W. Wlodarski, and M. K. Ghantasala, Sens. Actuators B **64**, 169 (2000).
[27] M. Musci, M. Notaro, F. Curcio, M. C. Casale, and G. De Michele, J. Mater. Res. **7**, 2846 (1992).
[28] M. Ocaña, V. Fornés, J. V. García-Ramos, and C. J. Serna, J. Solid State Chem. **75**, 364 (1988).
[29] G. A. Tompsett, G. A. Bowmaker, R. P. Cooney, J. B. Metson, K. A. Rodgers, and J. M. Seakins, J. Raman Spectrosc. **26**, 57 (1995).

[30] JCPDS, 43-1290 (1997).
[31] JCPDS, 09-0235 (1997).
[32] JCPDS, 44-1053 (1997).
[33] JCPDS, 37-1468 (1997).
[34] JCPDS, 39-1407 (1997).
[35] S. Bernal, F. J. Botana, J. J. Calvino, C. Lopez-Cartes, J. A. Perez-Omil, and J. M. Rodriguez-Izquierdo, Ultramicroscopy **72**, 135 (1998).
[36] A. Bokhimi Morales, O. Novaro, T. Lopez, E. Sanchez, and R. Gomez, J. Mater. Res. **10**, 2788 (1995).
[37] D. G. Isaak, J. D. Carnes, O. L. Anderson, H. Cynn, and E. Hake, Phys. Chem. Miner. **26**, 31 (1997).
[38] V. Swamy and L. S. Dubrovinsky, J. Phys. Chem. Solids **62**, 673 (2001).
[39] R. D. Shannon and J. A. Pask, J. Am. Ceram. Soc. **48**, 391 (1965).
[40] S. Hishita, I. Mutoh, K. Koumoto, and H. Yanagida, Ceram. Int. **9**, 61 (1983).
[41] M. C. Carotta, M. Ferroni, D. Gnani, V. Guidi, M. Merli, G. Martinelli, M. C. Casale, and M. Notaro, Sens. Actuators B **58**, 310 (1999).
[42] L. E. Depero, L. Sangaletti, B. Allieri, E. Bontempi, A. Marino, and M. Zocchi, J. Cryst. Growth **198/199**, 516 (1999).
[43] J. Marien, T. Wagner, G. Duscher, A. Koch, and M. Rühle, Surf. Sci. **446**, 219 (2000).
[44] U. Diebold, J.-M. Pan, and T. E. Madey, Phys. Rev. B **47**, 3868 (1993).
[45] B. Joyce, Vacuum Solutions **17**, 11 (2000).